GEOPHYSICS, VOL. 81, NO. 4 (JULY-AUGUST 2016); P. D293–D301, 15 FIGS., 1 TABLE.
10.1190/GEO2015-0476.1

Seismic velocities of halite salt: Anisotropy, heterogeneity, dispersion, temperature, and pressure effects

Fuyong Yan[1], De-hua Han[1], Qiuliang Yao[2], and Xue-Lian Chen[3]

ABSTRACT

We have made various experimental investigations on rock-physics properties of the halite salt coming from a salt dome in the U.S. Gulf Coast Basin. The effect of crystal defects and intercrystal cracks on the P-wave velocity of the halite salt sample can be mitigated after high-pressure annealing. The temperature effect on seismic velocities of halite salt is dominant relative to the stress effect. Azimuthal anisotropy is not observed on the halite salt samples. We have observed that the velocity variations in different directions were mostly caused by the crystal-scale heterogeneity. For the salt structures primarily made of creep-deformed halite, the effect of seismic velocity anisotropy might be negligible for seismic exploration. No significant dispersion of seismic velocities was observed from the low-frequency measurement. Our measurements supply basic information for seismic velocity model building that may help to improve seismic imaging of salt structures.

INTRODUCTION

Salt structures dominate the geologic features of the Gulf Coast Basin and play an important role in oil and gas exploration in the Gulf of Mexico area (Martinez, 1991). There are other salt basins in the world, such as the west African margin and the subsalt basins of the Brazilian margins, that are associated with significant petroleum discoveries (Leveille et al., 2011). Taking advantage of its excellent sealing properties, the salt structures can also be used to store petrochemicals and even hazardous materials, such as nuclear wastes (Thoms and Gehle, 2000). The salt structures are formed from the plastically deformed salt formation by rising buoyantly through the heavier sedimentary deposits. Therefore, the geometric shapes of salt structures are usually very complicated. The surrounding formation may be severely altered by the protruding salt structures, mechanically and geochemically. Formation of the salt structures is usually beneficial to the formation of the oil and gas traps, but it also poses great challenges in oil and gas exploration. The challenges come from the difficulty in delineating the geometry of the salt structure (Davison et al., 2013; Jones and Davison, 2014). A rational velocity model is a prerequisite for successful seismic imaging, but velocity model building remains the least well-addressed issue in contemporary seismic imaging today (Jones, 2010). In seismic imaging, the salt body is often assumed to be isotropic and homogeneous with constant velocities; the velocities of neighboring formations are also usually assumed to be unaffected by salt protrusion.

A naturally formed single halite crystal is usually cube shaped and has cubic velocity anisotropy (Sun, 1994). There are speculations that the salt bodies are anisotropic in seismic velocities because halite is usually a primary or dominant composition of the salt structures. Landrø et al. (2011) observe moderate velocity anisotropy in the salt outcrop at Cardona, Catalonia in Spain. The salt outcrop shows alternating clay-halite layers with thicknesses in the order of several millimeters. Therefore, the velocity anisotropy observed can be caused by the layered structure (Backus, 1962) or the intrinsic anisotropy of the clay layers. The salt anisotropy observed by Planchart (2014) from the vertical seismic profile (VSP) data may also be caused by the layered structures, because there are thin interbeds of calcareous shale, mudstone, sandstone, and siltstone. Vargas-Meleza et al. (2015) study the seismic anisotropic properties of various evaporates. Ultrasonic measurements are conducted on cube-shaped samples at room temperature, and no confining stress is applied. For halite-dominated salt, no clear evidence of seismic anisotropy is observed. There are other interpretations of seismic

Manuscript received by the Editor 8 September 2015; revised manuscript received 8 January 2016; published online 13 May 2016.
[1]University of Houston, Department of Earth and Atmospheric Sciences, Houston, Texas, USA. E-mail: yanfyon@yahoo.com; dhan@uh.edu.
[2]Formerly University of Houston, Department of Earth and Atmospheric Sciences, Houston, Texas, USA; currently Halliburton Consulting and Project Management, Houston, Texas, USA. E-mail: julian_yao@hotmail.com.
[3]China University of Petroleum, School of Geosciences, Qingdao, China. E-mail: chenxl@upc.edu.cn.

anisotropy from salt bodies (Kendall and Raymer, 1999; Raymer et al., 2000) based on the S-wave splitting phenomenon.

Velocity model building for seismic imaging should be based on field or laboratory measurements of the subsurface rocks. Despite the importance of salt rocks for petroleum exploration, laboratory measurement data on the rock-physics properties of the subsurface salt rocks are rare. Because the salt structures can occur in wide ranges of depths and temperatures, in this study, we will first try to measure the stress and temperature effects on seismic velocities of halite salt, and then we will investigate the existence of velocity anisotropy on the halite salt sample. Finally, low-frequency measurement is conducted to test the frequency dependency of seismic velocities.

SAMPLE DESCRIPTION AND PREPARATION

The halite core sample (Figure 1) comes from the Napoleonville salt dome, Assumption Parish, Louisiana, USA. The Napoleonville salt dome is a part of the Gulf Coast salt basin. The top of the salt dome is approximately 150 m below the surface, and the core samples come from a depth of approximately 300 m. The root of the salt dome is approximately 12,000 m deep (CB&I, 2013). The Napoleonville salt dome has been explored for brine mining and storage since 1950 (Nayak and Dreger, 2014). One of the salt caverns collapsed, and a large sinkhole was discovered on 3 August 2012. The sinkhole has developed into a lake with a surface area of approximately 20,000 m^2 and a maximum depth of 100 m. The primary goal of taking core samples from the subsurface is to study the mechanical properties of the salt for investigation of the sinkhole accident. The goal of our laboratory experiments is to study the rock-physics properties of halite salt.

Preparation of the cylindrical sample for laboratory measurement is more difficult for halite salt than other common sedimentary rocks. Although halite salt is unusually soft as a sedimentary rock (halite has a Mohs hardness of approximately 2–2.5), it is very brittle for shaping because the halite polycrystallines have dimensions of approximately 5–15 mm, which is much larger than the grains of common sedimentary rocks. To make a sample for traditional ultrasonic velocity measurement, we first cut the core into a gross cylindrical shape, and then used a metal lathe to shape it into a perfect cylinder. It is suggested that the metal lathe should be cleaned right after usage because the halite salt is very corrosive to common metal lathes. The cylindrical sample has a diameter of 3.8 cm and a length of approximately 5 cm. We also made a cubic sample with all the edges cut for velocity measurements in 45° with respect to the vertical direction. The halite sample has a glassy luster. The whitish spots indicate defects in the crystals or opening of intercrystal cracks. The bulk density of the halite is measured at 2.165 g/cm^3. The porosity is too low to be reliably measured by the helium porosity meter, and it is assumed to be zero.

Figure 1. (left) Halite salt core and (right) samples made from it for ultrasonic velocity measurement and low-frequency measurement.

CORE DAMAGE, HYSTERESIS, AND STRESS EFFECT

The core damage induced during the coring process can be observed from the whitish spots on the surface of the salt core (Figure 1). There may also be damage created during preparation of the sample for laboratory measurement. It is reported that due to plastic deformation, the damage may be recoverable by annealing under high pressure (Lebensohn et al., 2003). To observe the real stress effect on seismic velocities, we first need to stabilize the halite sample and let it partially recover from the damage induced by coring and sample preparation. In Figure 2, we monitor the P-wave velocity variations under three cycles of stress loading and unloading. Except of the first stress loading process, the stress effect on P-wave velocity is not significant. The velocity increasing during the first stress loading process may be primarily caused by closing of intercrystal cracks. Part of the intercrystal cracks may be annealed under high pressure, so the P-wave velocity cannot drop down to the initial low value when the pressure is decreased to the same level. Obvious hysteresis is observed, which may be related to plastic property of

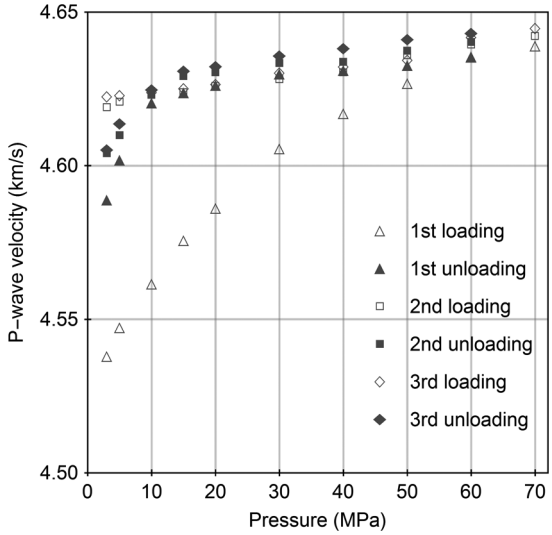

Figure 2. Initial stress effect observation and stabilization of the halite sample. For each cycle of stress loading and unloading, the pressure is first increased sequentially from 3 to 50 MPa, and then decreased sequentially to 3 MPa. The second cycle of stress loading and unloading is measured 12 h after the first circle, and the third cycle of stress loading and unloading is measured 24 h after the second circle. At the end of each cycle, the sample stays under a confining pressure of 3 MPa.

halite salt. There is a good repeatability between measurements of the second and third cycles of stress loading and unloading. After the sample is stabilized, the stress effect is not significant, which should be closer to the in situ conditions.

Figure 3 shows the halite sample after the initial stress effect measurement. The titanium buffers used in the ultrasonic velocity measurement have a Mors hardness scale of seven. The titanium is much harder than the halite salt, so there is an obvious pore pressure line pattern printed on the end surface of the halite sample, which causes the actual signal travel path be shortened by 0.1 mm. There is no observable diameter change on the sample. The pore pressure line pattern printed on the sample is rarely observed on similar measurements of common reservoir rocks. Based on this observation, it is speculated that the invading salt may be able to enter the macropores of the contacting sandstone and significantly increase seismic velocities.

TEMPERATURE AND STRESS EFFECTS

Salt bodies are distributed in a wide depth range from tens of thousands of meters to the surface. Therefore, it is necessary to know the effect of pressure and temperature on seismic velocities. Considering the limitation of the equipment, we set the pressure measurement range from 5 to 50 MPa, and the temperature measurement range from 23°C to 143°C. The central frequency of the piezoelectric transducer used for ultrasonic velocity measurement is approximately 1 MHz. Before measurements on the sample, the measurement system was calibrated at each pressure and temperature measurement point to be applied on the sample. The process of the ultrasonic velocity measurement on the halite sample is similar to that of the calibration process except that longer waiting time is needed at each measurement step to consider possible effects of hysteresis or creeping of the halite salt sample. At each temperature, we first increase the pressure to 50 MPa, and then decrease the pressure sequentially and record the traveltimes at each pressure. Then, we increase the temperature to the next level. After the temperature is stabilized, the pressure is increased to 50 MPa again, and the traveltimes are recorded when the pressure is decreased sequentially. The time of heating and velocity measurement for each temperature is approximately 2 h.

Figure 4 shows the measured effects of pressure and temperature on P- and S-wave velocities of the halite sample. It can be seen that in the temperature and pressure measurement ranges, the effect of temperature on seismic velocities is much stronger than pressure. At a confining pressure of 50 MPa, the P-wave velocity change between the lowest and highest measurement temperatures is 150 m/s (3.3%) and the S-wave velocity change is 90 m/s (3.6%). Including the stress effect, the maximum P-wave velocity change in the pressure and temperature measurement range is 170 m/s (3.9%) and the maximum S-wave velocity change is 110 m/s (4.3%). The measurement results are summarized in Table 1.

For practical application, we bring up the following empirical relations by nonlinear fitting of the measurement data:

$$V_P = 4.6910 - 0.01918e^{-0.05164P} + 1.3265 \times 10^{-6}PT - 0.001707T + 2.3893 \times 10^{-6}T^2, \quad (1)$$

$$V_S = 2.5830 - 0.03440e^{-0.2081P} + 9.8889 \times 10^{-7}PT - 0.0006058T - 9.6832 \times 10^{-7}T^2, \quad (2)$$

where P is the pressure in MPa and T is the temperature in °C. The R^2 regression coefficients are 0.999 and 0.992 for the V_P and V_S data, respectively. Figure 4 shows the measured data with the fitting models.

Compared with the ordinary sedimentary rocks, such as sandstones and carbonate rocks, the relative importance of temperature effect on the seismic velocities of halite salt is related to its special rock-physical proprieties. For sedimentary rocks, the stress effect on seismic velocities is mainly controlled by poroelasticity. For halite salt experiencing creep deformation, the stress effect is not significant because the porosity is negligible and the intercrystal cracks are

Figure 3. Print of pore pressure line pattern of (left) the buffer on the end surface of (right) the halite sample.

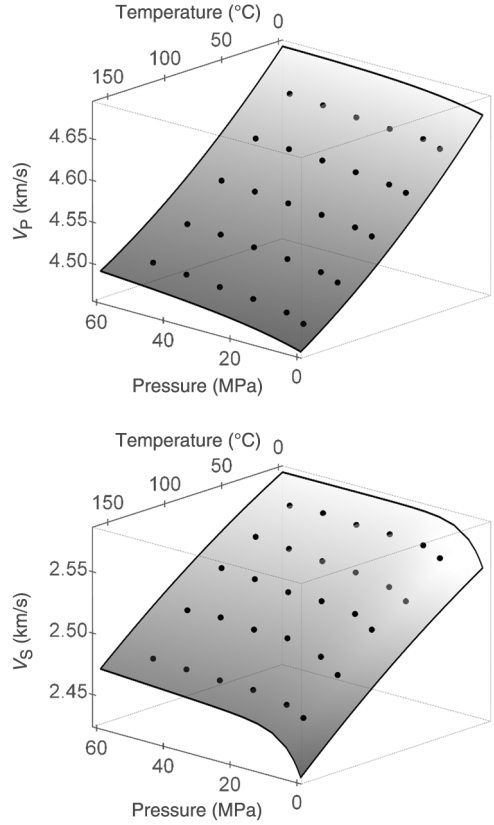

Figure 4. Effects of temperature and stress on P- and S-wave velocities. The velocities are measured at temperatures of 23°C, 53°C, 83°C, 113°C, and 143°C, and at pressures of 5, 10, 20, 30, 40, and 50 MPa.

not developed. The temperature effect on seismic velocities is related to temperature dependence of the crystal lattice strength. The melting point is an indication of the strength of the crystal lattice. The stronger the lattice, the higher is the melting point (Pandit, 2007). The temperature effect on seismic velocities of halite should be much stronger than common sedimentary rocks because halite has a much lower melting point than the common minerals in sedimentary rocks (halite, 801°C; calcite, 1339°C; and quartz, 1670°C; Hurlbut and Klein, 1985). Timur (1977) conducts an experimental study on the temperature dependency of seismic velocities in brine-saturated sandstones and carbonate rocks. For a 100°C increase in temperature, on the average, he observes a P-wave velocity decrease of 1.7% and an S-wave velocity decrease of 0.9%. Here, part of the P-wave velocity decrease is due to the brine property change. The corresponding P-wave velocity decrease we observed on the halite sample is 2.8% and the S-wave velocity decrease is 2.6%.

Figure 5 shows the effects of temperature and pressure on the dynamic Poisson's ratio. Generally, in the pressure and temperature measurement ranges, the variation of Poisson's ratio is not significant. At the same temperature, different circles represent Poisson's ratios at different pressures. It can be seen that the stress effect on Poisson's ratio is trivial and is masked by the measurement uncertainty. The temperature effect is not noticeable before 120°C, and there seems to be a slight increase in Poisson's ratio over 120°C.

CUBIC ANISOTROPY

The naturally formed halite crystal is cube-shaped and has cubic elastic anisotropy (Simmons and Wong, 1971; Sun, 1994). The halite salt from the Gulf of Mexico salt basin is usually very pure, and more than 95% of the composition is NaCl (Martinez, 1991). Therefore, it is suspected that elastic properties of the halite salt may be related to cubic elastic anisotropy. Cubic anisotropy is the simplest anisotropy determined by three independent elastic constants. The elastic tensor can be expressed by

$$\mathbf{C} = \begin{pmatrix} c_{11} & c_{12} & c_{12} & 0 & 0 & 0 \\ c_{12} & c_{11} & c_{12} & 0 & 0 & 0 \\ c_{12} & c_{12} & c_{11} & 0 & 0 & 0 \\ 0 & 0 & 0 & c_{44} & 0 & 0 \\ 0 & 0 & 0 & 0 & c_{44} & 0 \\ 0 & 0 & 0 & 0 & 0 & c_{44} \end{pmatrix}. \quad (3)$$

Figure 6 shows the coordinate systems of cubic anisotropy. The phase velocities in the plane determined by any two of the three principal axes can be expressed by (Tsang and Park, 1983)

$$V_{P\theta} = \sqrt{\frac{c_{11}+c_{44}+\sqrt{(c_{11}-c_{44})^2\mathrm{Cos}[2\theta]^2+(c_{12}+c_{44})^2\mathrm{Sin}[2\theta]^2}}{2\rho}}, \quad (4)$$

$$V_{SV\theta} = \sqrt{\frac{c_{11}+c_{44}-\sqrt{(c_{11}-c_{44})^2\mathrm{Cos}[2\theta]^2+(c_{12}+c_{44})^2\mathrm{Sin}[2\theta]^2}}{2\rho}}, \quad (5)$$

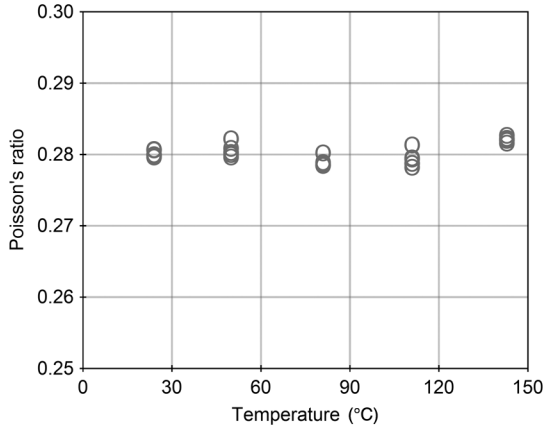

Figure 5. Effects of temperature and pressure on Poisson's ratio. At each temperature, there are six measurements on different pressures (5, 10, 20, 30, 40, and 50 MPa).

Table 1. Ultrasonic velocities (in units of km/s) of halite salt at different pressure and temperature conditions.

		Velocity (km/s) at different pressure (MPa)					
Temperature (°C)	Wave mode	5	10	20	30	40	50
23	P	4.637	4.643	4.644	4.647	4.651	4.654
	S	2.561	2.567	2.569	2.570	2.572	2.571
53	P	4.595	4.599	4.603	4.607	4.610	4.612
	S	2.531	2.539	2.544	2.546	2.548	2.551
83	P	4.556	4.562	4.566	4.569	4.572	4.575
	S	2.518	2.527	2.530	2.530	2.534	2.535
113	P	4.514	4.522	4.526	4.529	4.534	4.536
	S	2.491	2.502	2.509	2.509	2.512	2.510
143	P	4.480	4.488	4.493	4.497	4.501	4.504
	S	2.466	2.473	2.478	2.478	2.480	2.481

$$V_{\mathrm{SH}\theta} = \sqrt{\frac{c_{44}}{\rho}}, \tag{6}$$

where ρ is the bulk density. From equation 4, we have

$$V_{\mathrm{P}\theta 0} = V_{\mathrm{P}\theta 90} = \sqrt{\frac{c_{11}}{\rho}}, \tag{7}$$

$$V_{\mathrm{P}\theta 45} = \sqrt{\frac{c_{11} + 2c_{44} + c_{12}}{2\rho}}. \tag{8}$$

Here, the angle can be relative to any principal axes because the phase velocities are also symmetrical to the bisection of the two principal axes.

The general formulas for phase velocities at any directions other than the principal planes are more complicated and can be found in studies by Tsang and Park (1983) and Sun (1994). The minimum P-wave phase velocity is in direction [111], which has equal distances to the three principal axes:

$$V_{\mathrm{P}[111]} = \sqrt{\frac{c_{11} + 4c_{44} + 2c_{12}}{3\rho}}. \tag{9}$$

The velocity anisotropy based on Sun's (1994) measurement on a single pure halite crystal is shown in Figure 8. Based on Sun's (1994) measurement data, $V_{\mathrm{P}[001]} = 4.66$ km/s, $V_{\mathrm{P}[011]} = 4.45$ km/s, and $V_{\mathrm{P}[111]} = 4.37$ km/s. The P-wave anisotropy is approximately 6.2%. This should be the maximum possible P-wave anisotropy for halite salt when all the halite crystals are perfectly aligned in all the three principal axes. Based on equations 4–7, Figure 7 shows the phase velocities of a halite crystal in any of the principal planes. From Figure 7, the S-wave anisotropy is much stronger than P-wave anisotropy. It is also noted that in the direction where the P-wave velocity is minimum, the SV-wave velocity is maximum. In practices of seismic exploration, the S-wave information is usually less useful than the P-wave information due to its relative poor quality. In addition, S-wave velocity measurement has much higher uncertainty, so we only concentrate on P-wave anisotropy in this study.

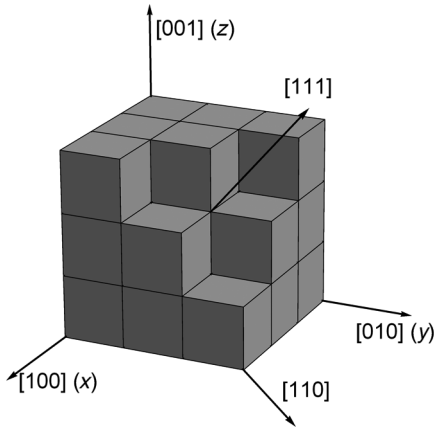

Figure 6. The coordinate systems (Miller index system and x-y-z system) for cubic anisotropy.

VELOCITY ANISOTROPY OR HETEROGENEITY

Our first attempt is to cut a cube from the halite core, with one of the normal directions of the cube parallel to the axial direction of the halite core. The side length of the cube is 3 cm. Next, we cut each

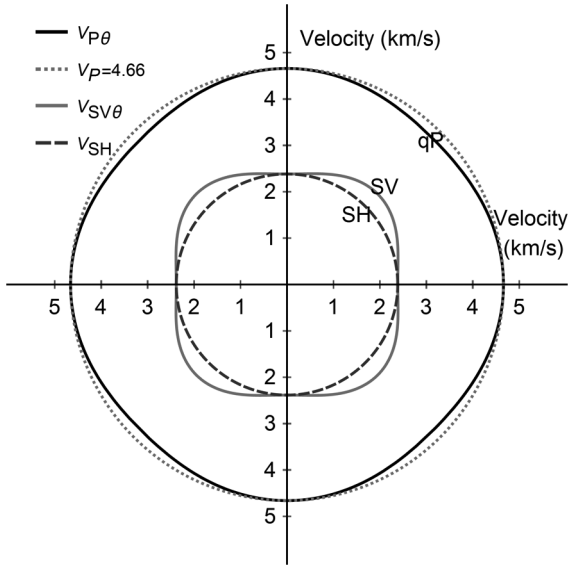

Figure 7. Phase velocities of a halite crystal in the principal planes. Parameters used for plotting: $c_{11} = 47.0$, $c_{12} = 12.3$, and $c_{44} = 12.3$ GPa; data from Sun (1994).

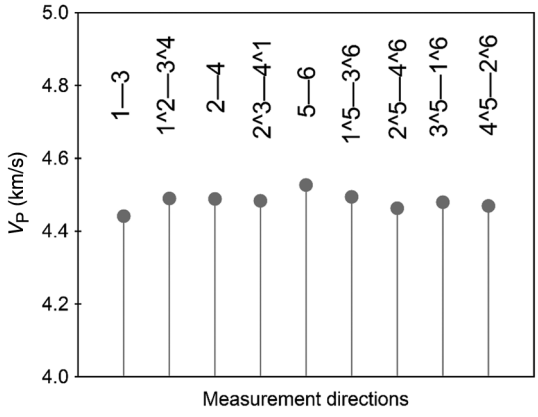

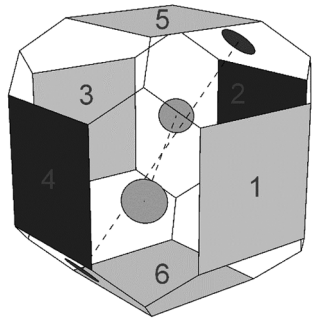

Figure 8. P-wave velocities measured from the cubic halite sample (above) with edges cut and (below) the diagram of the halit sample.

edge of the cube to form more planes for velocity measurement (as shown in the right bottom panel of Figure 1). The angle between the new oblique plane and the neighboring cubic plane is 45°. The measurement is conducted on benchtop. The central frequency of the piezoelectric transducer is approximately 1 MHz. The upper panel of Figure 8 shows the measured P-wave velocities at different directions. Here, 1–6 refers to the surfaces of the original cube, 1–3 denotes the normal travel path from surface 1 to surface 3, and 2^5–4^6 denotes the normal travel path from the oblique plane between surfaces 2 and 5 to the oblique plane between surfaces 4 and 6. For a clear illustration of the directions where the velocities are measured, the diagram of the cubic sample with the edges cut is shown in the lower panel of Figure 8. We only know that 5–6 is in the vertical direction. The maximum velocity occurs in the vertical direction. The maximum P-wave velocity variation among these measurements is 2.0%, which is noticeably smaller than the cubic anisotropy based on measurement of a single halite crystal. Therefore, the connection between the observed velocity variation and cubic velocity anisotropy is not clear, and more measurements at different directions are needed to confirm the connection.

We designed a benchtop rotational velocity measurement system (Yan et al., 2014). Figure 9 shows the diagram of rotational group velocity measurement on a cylindrical halite sample. The halite sample can be rotated to any angle in the tube pinned with an angle panel at the end surface. A group velocity is measured because in the cross section, the contact between the buffer and halite sample can be approximated as a point (Yan et al., 2014). This halite sample is the same sample used for measurement of the stress and temperature effects on the ultrasonic velocities. To test for possible velocity anisotropy, we plan to measure the velocity variations in the transversal directions at circles A and B (as shown in Figure 10). The hypothesis is that if the velocity variation patterns at circles A and B are similar, then there may be velocity anisotropy.

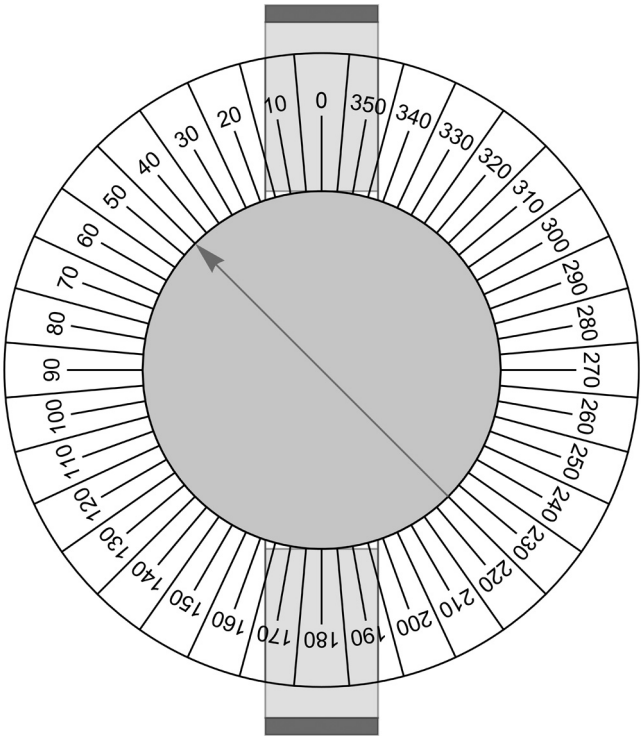

Figure 9. Diagram of rotational group velocity measurement on a halite salt sample. The sample is in a tube pinned with an angle panel. The arrow denotes the arbitrary 0° direction marked on the end surface of the halite sample.

Figure 11 shows the signal traces recorded from 0° to 180° along circle A. The 0° direction is arbitrary and same for circles A and B. Most of the traces have clear first-arrival wave signals, but they are not consistent in waveforms and some traces are much noisier than the other traces. We check the sample and find that the nosier traces come from the directions passing part of the sample that may be slightly damaged, as can be seen from the whitish spots in the upper part of the halite sample in the left panel of Figure 10. Indeed the sample was accidentally dropped on the desktop before the rotational group velocity measurement and small pieces of halite crystals were found to fall off from the sharp edge. To mitigate the effect of the damaged part on velocity measurement, we put the sample in a pressure vessel and let it stay under 60 MPa for 5 h, and then we took it out. As shown in Figure 10, the color of the damaged part

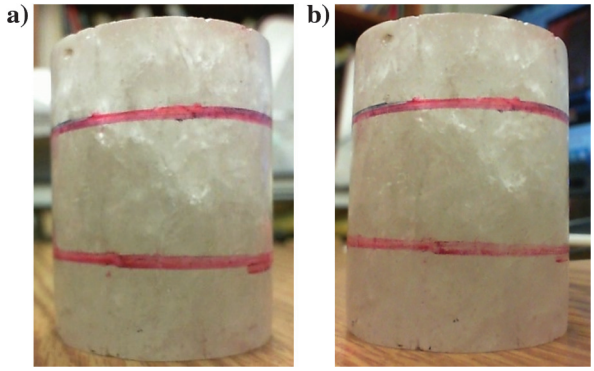

Figure 10. Comparison of the halite sample (a) before and (b) after high-pressure annealing. The pictures are taken approximately in the same direction. The whitish upper part indicates the damage from falling on the desktop. The red circles (top A and bottom B) mark positions of ultrasonic measurements.

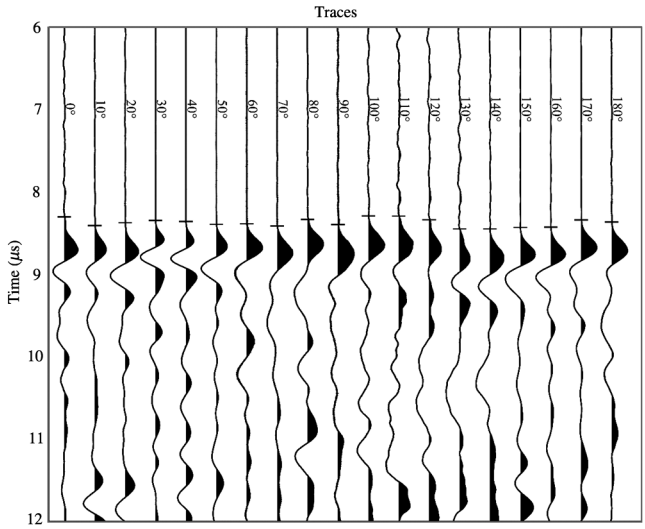

Figure 11. P-wave signal traces at different azimuths around circle A before high-pressure annealing. The short bars around the first-arrival signals denote the first break times picked.

becomes less whitish, and the sample seems to be partially recovered or annealed under high pressure. We did the rotational group velocity measurement again at the same rotational position (circle A). Figure 12 shows a comparison of the P-wave signal traces before and after high-pressure annealing. It can be seen that after high-pressure annealing, waveforms of the first-arrival signals are more consistent, and the traces before the first-arriving signals are cleaner for the measurements passing through the damaged parts and the first-arrival signals arrive earlier. Therefore, the ultrasonic velocity measurement reveals that the damaged sample is partially recovered. An implication of the observed high-pressure annealing phenomenon is that the subsurface salt cannot sustain substantial differential stress, and there should be no fractures within the salt bodies in the geologic time scale.

The distance between circles A and B in axial direction is approximately 2 cm. If there is significant velocity anisotropy, we should be able to observe a similar azimuthal velocity variation pattern at circle B. Figure 13 shows a comparison of the P-wave signal traces at these two locations. After high-pressure annealing, all the P-wave traces have consistent first-arrival waveforms, the quality of the received P-wave signals is excellent. The P-wave signal arrivals are slightly earlier in some directions than others, and the variation patterns at circles A and B are not consistent, which means that azimuthal P-wave anisotropy is not observed on this sample.

Figure 14 shows the measured azimuthal P-wave velocities at circles A and B. On the real scale polar plot, the azimuthal variation of P-wave velocity is insignificant, and the velocity differences between P-wave velocities measured on circles A and B are small in some directions and almost indiscernible in other directions. In the polar plot with magnified radius scale, we can see that the maximum velocity variation is approximately 150 m/s (or 3%), but the velocity variation pattern at circles A and B are obviously different, so there is not even weak anisotropy observed. The azimuthal velocity variation is noticeably greater than the measurement uncertainty (less than 1%). The difference may be caused by heterogeneity of the halite crystals, which have different sizes and the crystal lattices may orientate in different directions due to a long distance of transportation from where the evaporate is originally deposited. Zong (2014) makes azimuthal P- and S-wave velocity measurements on a halite sample from the same area. She did not repeat the measurements on different locations of the sample as we showed here. The P-wave azimuthal variation from her measurement is approximately 2%, and the S-wave azimuthal variation is approximately 5%. It is found that the direction of the maximum P-wave velocity is consistent with the direction of the maximum S-wave velocity, which is not an indication of cubic anisotropy. As shown in Figure 7, the direction of the minimum P-wave velocities corresponds to the direction of the maximum SV-wave velocity. Therefore, even if there exists seismic velocity anisotropy from Zong (2014) measurement, it may not be caused by the cubic anisotropy of the halite crystals.

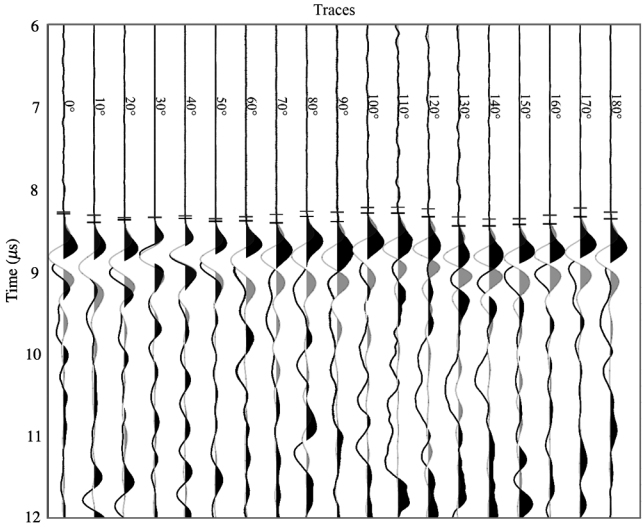

Figure 12. Comparison of P-wave signal traces at different azimuths around circle A before (black) and after (gray) high-pressure annealing. The short bars around the first-arrival signals denote the first break times picked. After high-pressure annealing, the waveforms are more consistent. The noiser traces due to sample damage become cleaner after high-pressure annealing and the first break times arrive earlier.

LOW-FREQUENCY MEASUREMENT

Imaging around the creeping deformed salt is one of the most challenging tasks in seismic imaging. Because the salt is plastic in a geologic time scale, it is suspected that the poor imaging around and inside of the salt may be related to significant attenuation of the seismic wave energy by the salt body. Therefore, we have conducted velocity dispersion measurement on the halite salt sample using the low-frequency system built by our laboratory (Yao, 2013). The principles of low-frequency measurement can be found in the works of Spencer (1981) and Batzle et al. (2006). The samples are stuck together with a metal standard that is assumed perfectly elastic, and they are forced to vibrate at different frequencies. Strain gauges are attached on the cylindrical surfaces of the metal standard and the sample to measure the longitudinal strain and radial strain. The Young's modulus and Poisson's ratio can be calculated from the strains in different directions. The P- and S-wave velocities are calculated from Young's modulus and Poisson's ratio. Attenuation

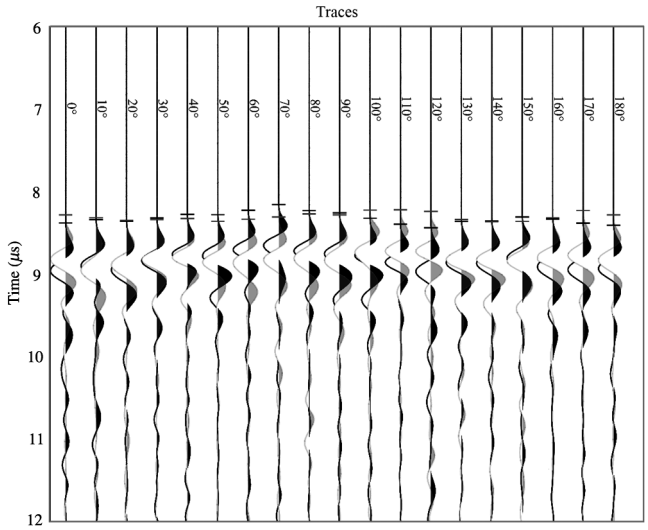

Figure 13. Comparison of P-wave signal traces at different azimuths at position A (gray) and position B (black). The short bars around the first-arrival signals denote the first break times picked.

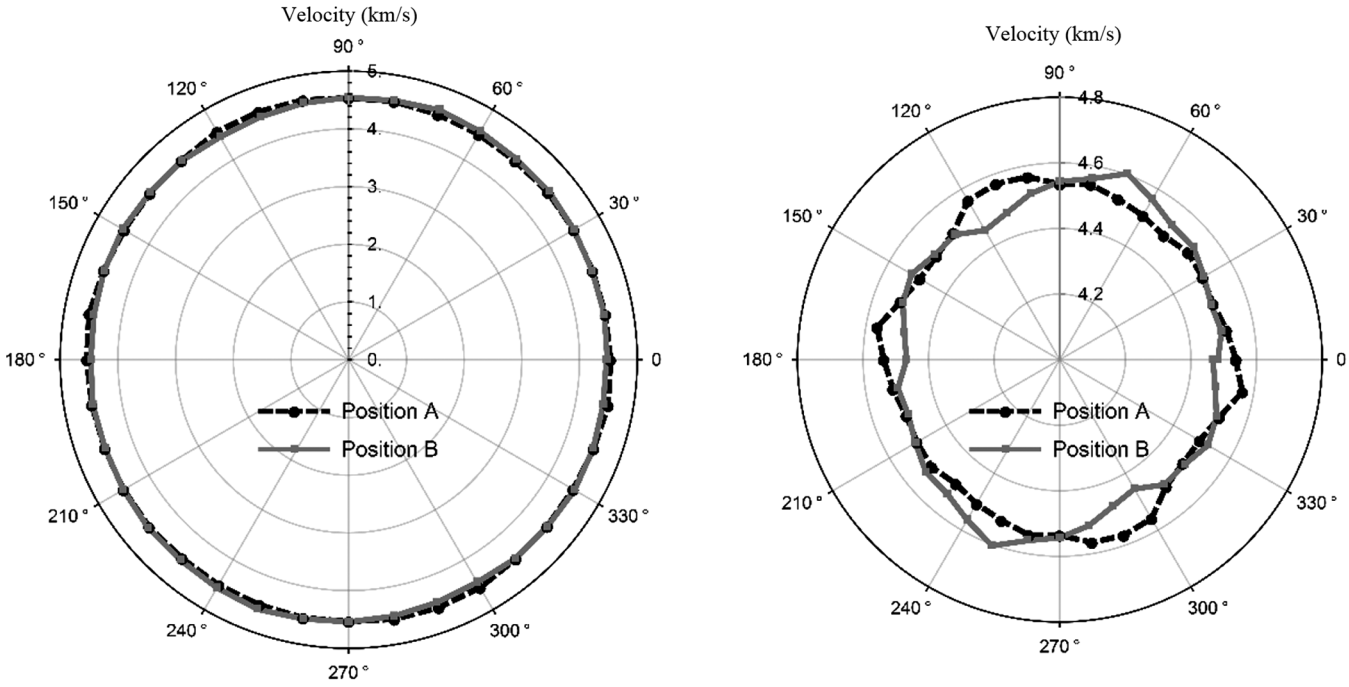

Figure 14. Comparison of P-wave velocities at different azimuths around positions A and B. No consistent velocity anisotropy is observed (left: real scale polar plot and right: radius-magnifed polar plot).

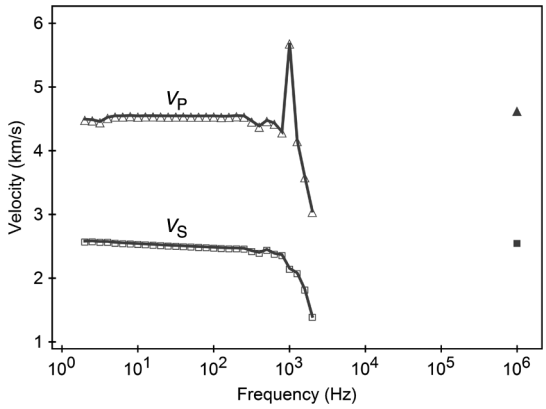

Figure 15. Dispersions of halite seismic velocities from low-frequency measurement. The fluctuations approximately 10^3 Hz are due to resonance of the measurement system and the affected data points are not reliable. The two data points at 10^6 Hz are from the ultrasonic measurements (at 23°C, 5 MPa).

is estimated from the phase difference of the strain variation on the metal standard and the sample.

The measurement is conducted at room temperature and pressure conditions. As shown in Figure 15, in seismic frequency range, the P-wave velocity has no trend of increasing with frequency and the S-wave velocity even slightly decreases with frequency, which may be caused by measurement uncertainty. At more than 1000 Hz, the measurement results begin to be affected by the resonance vibration of the system and are not reliable. The P-wave velocities measured at seismic frequency ranges are approximately equal to the average velocity measured from the ultrasonic measurements (Figure 8), so there should be no significant dispersion of P-wave velocity at the frequency range between seismic frequency and ultrasonic frequency. There is a causal relation between attenuation and dispersion of seismic waves, so there should be no significant attenuation as well.

CONCLUSION

The temperature effect on seismic velocities of halite salt is dominantly relative to the stress effect. For laboratory measurement of the elastic properties of salts, it is important to check possible damage of the salt sample, and let the sample stay at the subsurface in situ stress condition for a certain time to recover from possible damage. We did not observe azimuthal anisotropy on the halite salt samples. The velocity variations in different directions observed in laboratory are most likely caused by crystal-scale heterogeneity, the velocity anisotropy of halite salt experienced significant creeping deformation should be negligible for seismic exploration. No significant dispersion of seismic velocities is observed from the low-frequency measurement.

ACKNOWLEDGMENT

We thank the Fluid/DHI Consortium sponsors for financial support. We thank K. Katahara for many beneficial discussions. Especially, we thank Allied Geophysical Laboratory in University of Houston for providing the halite sample.

REFERENCES

Backus, G. E., 1962, Long-wave elastic anisotropy produced by horizontal layering: Journal of Geophysical Research, **67**, 4427–4440.

Batzle, M. L., D.-H. Han, and R. Hofmann, 2006, Fluid mobility and frequency-dependent seismic velocity — Direct measurements: Geophysics, **71**, no. 1, N1–N9, doi: 10.1190/1.2159053.

Chicago Bridge & Iron Company (CB&I), 2013, Blue Ribbon Commission initial technical briefing, Louisiana State University, http://dnr.louisiana.

gov/assets/OC/BC_All_Updates/Plans_Reports/BlueRibb.04.05.13.pdf, accessed September 2015.
Davison, I., I. F. Jones, and D. Waltham, 2013, Seismic imaging of salt diapirs: Problems and pitfalls: Presented at the 13th International Congress of the Brazilian Geophysical Society, 1332–1336.
Hurlbut, C. S., and C. Klein, 1985, Manual of mineralogy, 20th ed.: John Wiley and Sons.
Jones, I. F., 2010, An introduction to velocity model building: EAGE.
Jones, I. F., and I. Davison, 2014, Seismic imaging in and around salt bodies: Problems and pitfalls: 84th Annual International Meeting, SEG, Expanded Abstracts, 3684–3687.
Kendall, R. R., and D. G. Raymer, 1999, Processing and interpretation of VSP data to determine salt anisotropy — Manogany Field, Gulf of Mexico: 61st Annual International Conference and Exhibition, EAGE, Extended Abstracts.
Landrø, M., C. Puigdefabregas, and B. Arntsen, 2011, Anisotropy in the salt outcrop at Cardona, Catalonia — Implications for seismic imaging: First Break, **29**, 41–45, doi: 10.3997/1365-2397.2011022.
Lebensohn, R. A., P. R. Dawson, D. H. Kern, and H.-R. Wenk, 2003, Heterogeneous deformation and texture development in halite polycrystals: Comparison of different modeling approaches and experimental data: Tectonophysics, **370**, 287–311, doi: 10.1016/S0040-1951(03)00192-6.
Leveille, J. P., I. F. Jones, Z.-Z. Zhou, B. Wang, and F. Liu, 2011, Subsalt imaging for exploration, production, and development: A review: Geophysics, **76**, no. 3, WB3–WB20, doi: 10.1190/geo2011-0156.1.
Martinez, J. D., 1991, Salt dome: American Scientist, **79**, 420–431.
Nayak, A., and D. S. Dreger, 2014, Moment tensor inversion of seismic events associated with the sinkhole at Napoleonville salt dome, Louisiana: Bulletin of the Seismological Society of America, **104**, 1763–1776, doi: 10.1785/0120130260.
Pandit, N. K., 2007, Introduction to the pharmaceutical sciences: Lippincott Williams & Wilkins.
Planchart, C., 2014, Estimation of salt anisotropy using zero offset, walkaway and walkaround VSP data from the Red Sea, Saudi Arabia: A case study: 84th Annual International Meeting, SEG, Expanded Abstracts, 389–392.
Raymer, D. G., J.-M. Kendall, D. Pedlar, R. R. Keiidall, M. C. Mueller, and G. J. Beaudoin, 2000, Seismic anisotropy in salt bodies — Implications for seismic imaging: 62nd Annual International Conference and Exhibition, EAGE, Extended Abstracts.
Simmons, G., and H. Wong, 1971, Single crystal elastic constants and calculated aggregate properties: A handbook: MIT Press.
Spencer, J. W., 1981, Stress relaxations at low frequencies in fluid saturated rocks: Attenuation and modulus dispersion: Journal of Geophysical Research, **86**, 1803–1812, doi: 10.1029/JB086iB03p01803.
Sun, Z., 1994, Seismic anisotropy in salt from theoretical study, modeling, and field experiments: Master's thesis, University of Calgary.
Thoms, R. L., and R. M. Gehle, 2000, A brief history of salt cavern use, *in* R. M. Geertman, ed., Proceedings of the 8th World Salt Symposium, Part I: Elsevier B.V., 207–214.
Timur, A., 1977, Temperature dependence of compressional and shear wave velocities in rocks: Geophysics, **42**, 950–956, doi: 10.1190/1.1440774.
Tsang, T., and H.-Y. Park, 1983, Sound velocity anisotropy in cubic crystals: Physics Letters, **99**, 377–380, doi: 10.1016/0375-9601(83)90297-9.
Vargas-Meleza, L., D. Healy, G. I. Asop, and N. E. Timms, 2015, Exploring the relative contribution of mineralogy and CPO to the seismic velocity anisotropy of evaporates: Journal of Structural Geology, **70**, 39–55, doi: 10.1016/j.jsg.2014.11.001.
Yan, F., D.-H. Han, and Q. Yao, 2014, Benchtop rotational group velocity measurement on shales: 84th Annual International Meeting, SEG, Expanded Abstracts, 2983–2986.
Yao, Q., 2013, Velocity dispersions and wave attenuation in reservoir rocks: Ph.D. thesis, University of Houston.
Zong, J., 2014, Elastic properties of salt: Laboratory measurements, well-log analysis, and a seismic survey over the Hockley salt mine, Texas: Master's thesis, University of Houston.